A Criterion for the Passivity of Haptic Devices

N. Diolaiti
DEIS, University of Bologna
V. Risorgimento 2, I-40136 Bologna
ndiolaiti@deis.unibo.it

G. Niemeyer
Telerobotics Lab
380 Panama Mall, Stanford, CA 94305
gunter.niemeyer@stanford.edu

F. Barbagli and J. K. Salisbury
AI-Robotics Lab
353 Serra Mall, Stanford, CA 94305
{barbagli, jks}@robotics.stanford.edu

***Abstract*— Rendering a stiff virtual wall remains a core challenge in the field of haptics. A passivity study of this problem is presented, which relates the maximum achievable wall stiffness to the system discretization and sampling delays, to the quantization of the encoder, to the inertia of the haptic device, as well as to both the natural viscous and Coulomb damping present in the haptic device. The resulting stability criterion generalizes previously known results. Its analytic derivation is verified in both simulation and experiments on a one degree of freedom testbed.**

***Index Terms*— Haptic Interfaces, Quantization, Coulomb Friction, Passivity, Virtual Walls**

I. Introduction

The aim of haptic interfaces is to render the mechanical features of simulated objects on the user, thus allowing a sensation of contact that would normally be experienced when physically interacting with real objects.

To achieve a good degree of *transparency*, several issues have to be taken into account in the design of a haptic interface. For instance, the mechanical device should exhibit low inertia and friction so that the user's perception is not affected by its dynamics [1] and a suitable trade-off between the number of actuated and sensed degrees of freedom (DOF) has to be devised depending on the particular application [2].

From the control perspective, other factors have to be carefully considered. Stiff virtual walls are commonly implemented by means of a digital control loop. This necessitates time-discretization as well as quantization of the sensed position, stemming from the limited encoder resolution, and of the commanded force, due to the D/A converter resolution. When a stiff virtual object has to be rendered, these non-idealities, together with the limited bandwidth of the actuation system, can lead to unstable or oscillatory behaviors that destroy the virtual reality illusion and may even be harmful to the operator.

Passivity theory has been used in [3], [4] as the main tool to provide stability conditions for a haptic display interacting with a human operator. The operator has also been described by passive but otherwise unknown elements [5]. In particular, several previous works [6], [7] have noted that the time delay introduced by the zero-order-hold has the effect of injecting (*generating*) energy into the system, in an amount proportional to the stiffness of the virtual object. If the intrinsic friction of the device is not sufficient to dissipate the excess energy, the interface becomes unstable. In [8] this concept has been exploited and generalized to the interaction with complex virtual environments, accounting for computational delays and different local models.

Much effort [9]–[11] has gone toward increasing the stiffness of virtual objects without undermining the stability of the overall system. However, the design of more effective control strategies requires a preliminary study on the stability of a haptic display accounting for all phenomena affecting the energy generation and dissipation while rendering stiff objects. A more complete picture of the system can facilitate the design of better mechanical structures, including appropriate dimensioning of the sensors and actuators. Similarly, results should predict the maximum stiffness that can be displayed by existing devices.

Beyond time discretization, stability may be impacted by quantization in the sensing/actuation system and by the limited bandwidth of the current amplifier. This paper analyzes the stability of a digital control loop in presence of quantization noise. In comparison to previous works, the nonlinearity represented by dynamic Coulomb friction is considered together with viscous friction and it is shown to be essential to avoid oscillations caused by quantization. The paper is organized as follows: in Sec. II the basic notation is introduced and the main passivity criterion is stated and discussed. Simulation results to validate to the criterion are given in Sec. III. The analytical proof is provided in Sec. IV where a detailed discussion on the energetic behavior of digital springs is included. Sec. V presents the experimental results obtained on a simple 1 DOF device, while final remarks and future work are discussed in Sec. VI.

II. Main Results

Most commonly haptic displays must render the stiffness of virtual objects, as sketched in Fig. 1, where a 1 DOF device is depicted. The mechanical structure is characterized by the inertia m, the viscous friction b and the dynamic Coulomb friction c; F_H is the force applied by the human operator while F_V is the force exerted by the

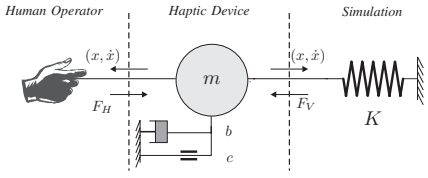

Fig. 1. Stiffness rendering by means of a haptic device

control system that simulates a virtual wall of stiffness K. Finally x and $\dot{x}$ are the position and the velocity of the device.

However, the haptic rendering is implemented by means of components that can only approximate the scheme of Fig. 1 and the deviation (non-ideality) introduced by each component along the control loop has to be analyzed in order to prevent oscillatory or unstable behaviors. As shown in Fig. 2, beside the time delay related to the discretization process, the quantization introduced by the position sensor or by the D/A converter, whose resolution is substantially higher, and the dynamics of the actuation subsystem cause the force F_V to be different from the force that a physical unilateral spring would exert.

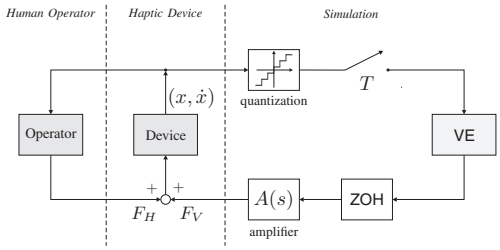

Fig. 2. Block scheme of the human interaction with a digital spring

A. Problem Statement

With reference to the block scheme of Fig. 2, the motion of the haptic device, modeled as a point-mass, is described by the following differential equation:

$$m\ddot{x}(t) + b\dot{x}(t) + c\,\mathrm{sgn}\left(\dot{x}(t)\right) = F_H(t) + F_V(t) \quad (1)$$

where b and c are the viscous and the dynamic Coulomb friction coefficients. If the actuator dynamics is fast enough to be ignored, the force exerted by the control system simulating a linear spring for positive displacements:

$$F_V(t) = -K\Delta\left(\left\lfloor \frac{x(hT)}{\Delta} \right\rfloor + \frac{1}{2}\right) \quad \forall t \in [hT, (h+1)T[,\ h \in \mathbb{N} \quad (2)$$

where T is the sampling time, h the discrete time variable, and Δ is the sensor resolution for the device. The notation $\lfloor . \rfloor$ is used to refer the integer part. The addition of the bias of $\frac{1}{2}\Delta$ creates a virtual force symmetric about the origin and bounds the position measurement error by $\frac{1}{2}\Delta$.

The main purpose of our analysis is to relate the displayed stiffness K to the behavior of the haptic device and to identify what parameters of the system have to be adjusted in order to achieve a *passive* interaction with the human operator. For this reason, it is particularly useful to try to reduce the number of parameters appearing in (1) by carrying out a dimensionless analysis. In particular, if we assume a dimensionless position ξ and time τ:

$$\xi := \frac{x}{\Delta} \qquad \tau := \frac{t}{T} \quad (3)$$

and if we agree that $\dot{\xi}(\tau) = d\xi(\tau)/d\tau$, the dimensionless velocity and acceleration are:

$$\dot{x}(t) = \frac{\Delta}{T}\dot{\xi}(\tau) \qquad \ddot{x}(t) = \frac{\Delta}{T^2}\ddot{\xi}(\tau) \quad (4)$$

while dimensionless forces φ_H and φ_V are obtained dividing by $K\Delta$, in particular:

$$\varphi_V(\tau) := \frac{F_V(\tau)}{K\Delta} = -\left(\lfloor \xi(h) \rfloor + \frac{1}{2}\right) \quad \forall \tau \in [h, (h+1)[,\ h \in \mathbb{N} \quad (5)$$

Therefore, the differential equation (1) can be rewritten as:

$$\mu\ddot{\xi}(\tau) + \beta\dot{\xi}(\tau) + \sigma\,\mathrm{sgn}\left(\dot{\xi}(\tau)\right) = \varphi_H(\tau) + \varphi_V(\tau) \quad (6)$$

whose dimensionless parameters are defined as:

$$\mu := \frac{m}{KT^2} \qquad \beta := \frac{b}{KT} \qquad \sigma := \frac{c}{K\Delta} \quad (7)$$

B. Passivity Criterion

The dimensionless formulation emphasizes that the system dynamics is governed by certain ratios between the parameters instead of the value of each single parameter. In particular, μ is proportional to the natural frequency $\omega_n = \sqrt{K/m}$ of the physical system and to the sampling frequency $\omega_s = 2\pi/T$; and the Nyquist condition to avoid aliasing $\omega_s \gg 2\omega_n$, corresponds to $\mu \gg 1/\pi^2$. On the other hand, the actual power dissipation does not depend only on b and c but on their ratios with respect to the parameters related to energy generation (see Sec. IV): the rendered stiffness K, the sampling time T and the resolution Δ. For this reason β and σ can be interpreted as *effective friction coefficients* and it can be proved that, if the inequality:

$$\left(\beta - \frac{1}{2}\right) + \left|\dot{\xi}(\tau)\right|^{-1}\left(\sigma - \frac{1}{2}\right) \geq 0 \qquad \forall \tau > 0 \quad (8)$$

holds, the haptic rendering of a wall of stiffness K, and consequently the whole haptic display, is passive [8], [12].

Note that (8) does not depend on μ since a mass does not generate nor dissipate energy, and on the force φ_H exerted by the human operator, since he is an external system with respect to the haptic device and cannot affect its passivity. Moreover, it can be argued that at frequencies above approximately 10 Hz, the human operator is incapable of controlling the interaction impedance and can only present stiffness together with substantial damping to the haptic device. Therefore the operator helps recover stability, dissipating excess energy and dampening vibrations or limit cycles and, from this point of view, the worst case is when the human input φ_H is null.

The inequality (8) can be seen as a generalization of Colgate's inequality [3] ($\beta > 1/2$ in the dimensionless formulation) to include dynamic Coulomb friction and sensor quantization. Graphically it translates to areas of the (β, σ) plane for which the overall system has different behaviors. Passivity is guaranteed only for points on the right of the critical line:

$$\sigma = \frac{1}{2} - \left|\dot{\xi}(\tau)\right|\left(\beta - \frac{1}{2}\right) \quad (9)$$

having slope $-|\dot{\xi}(\tau)|$ and rotating, counterclock-wisely as the velocity decreases, about the point $(1/2, 1/2)$. This line is vertical when $\dot{\xi}(\tau)$ tends to infinity, while it is horizontal when it tends to zero. This agrees with the

physical intuition, since the instantaneous power dissipation provided by the dynamic Coulomb friction is larger than the viscous dissipation at low velocities ($|\dot{\xi}(\tau)| \ll \sigma/\beta$), while at high velocities the situation is inverted. According

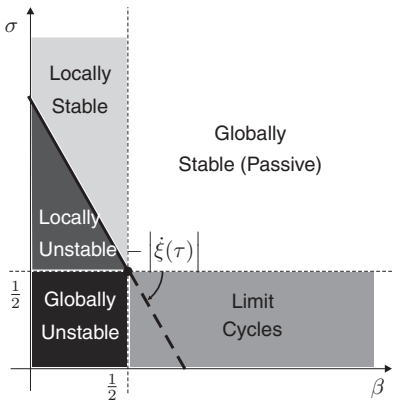

Fig. 3. Stability regions of the (β, σ) plane.

to this result, the behaviors of the haptic display can be classified depending on the values of β and σ, identifying four different regions in the (β, σ) plane (Fig. 3):

a) $\beta > \frac{1}{2}$, $\sigma > \frac{1}{2}$: points belonging to this region are characterized by high values of effective friction and are guaranteed to be passive regardless the initial conditions; the system is therefore globally stable (provided that the human operator is passive [5] as well).

b) $\beta < \frac{1}{2}$, $\sigma < \frac{1}{2}$: on the opposite of previous case, the dissipation is never sufficient to dissipate energy excess generated by the control algorithm and the system becomes unstable (in the sense that at least a passive human operator exists that cannot dissipate the extra-energy generated).

c) $\beta > \frac{1}{2}$, $\sigma < \frac{1}{2}$: this region gives rise to stable self-sustained oscillations (limit cycles). Decaying velocities $\dot{\xi}(\tau)$ rotate line (9) counter clockwise and prevent points from staying to the right of the line. In turn this prevents velocities from decaying further and generates energy to sustain the oscillations.

d) $\beta < \frac{1}{2}$, $\sigma > \frac{1}{2}$: in this case the stability of the system depends on the initial velocity $\dot{\xi}(0)$. Indeed, if (8) is satisfied at time $\tau = 0$, the system dissipates energy and the critical line rotates counterclock-wisely until the equilibrium is reached. On the contrary, if at time $\tau = 0$ the characteristic point is on the left of the critical line, the energy of the overall system increases leading to instability because the line rotates clock-wisely.

Because of this last observation, condition (8) can be simplified to:

$$\left(\beta - \frac{1}{2}\right) + \left|\dot{\xi}(0)\right|^{-1} \left(\sigma - \frac{1}{2}\right) \geq 0 \qquad (10)$$

i.e. by using the initial velocity of the system as opposed to the velocity at a generic time τ. By recalling the definitions (7) and (4), the passivity criterion can be rewritten as:

$$\left(b - \frac{KT}{2}\right) + |\dot{x}(0)|^{-1} \left(c - \frac{K\Delta}{2}\right) \geq 0 \qquad (11)$$

Moreover, on the (β, σ) plane it is possible to evaluate the impact of technological parameters, e.g. encoder resolution Δ and sampling time T stability of a haptic display given a stiffness level K. Indeed, since both β and σ depend on K in the same way, a stiffness increase moves the characteristic point along a line, as shown in Fig. 4 for P_1 and P_2. On the other hand, an increase

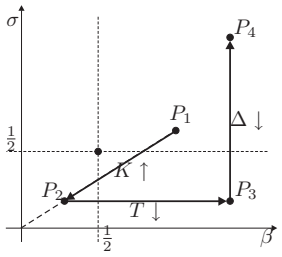

Fig. 4. Effects of variations of wall stiffness K, sampling time T and encoder resolution Δ on the (β, σ) plane.

of the sampling frequency moves the point to the right horizontally (P_2 to P_3) and a reduction of Δ corresponds to a vertical movement (P_3 to P_4), thus improving the stability of the overall system. Finally, because of (4), given a physical velocity $\dot{x}(t)$, the dimensionless velocity $\dot{\xi}(\tau)$, and therefore the slope of the critical line, depends on the ratio T/Δ.

III. Simulations

Before providing analytical proof of the passivity criterion (10), simulation results are shown in order to evaluate its accuracy. According to previous considerations, the dimensionless model (6) has been simulated assuming no initial deflection $\xi(0) = 0$, different initial velocities $\dot{\xi}(0)$ and a null input from the human operator. Several points of the (β, σ) plane have been simulated and the state vector $(\xi, \dot{\xi})$ has been evaluated for $\tau \in [0, 5 \times 10^4]$ corresponding to $t = 50$ sec. with a sampling time $T = 1$ ms, to determine the stability for each couple of values of β and σ. In Fig. 5(a) the results obtained with $\mu = 50$ and four different initial velocities are shown. The shaded areas, ranging from black to light gray represent, for each initial velocity, the regions of unstable behavior; the irregular profile is due to the discrete number of points that have been simulated. The critical lines associated to each case are dashed, while the dash-dot lines are used to identify the four regions of Fig. 3. A good correspondence between the predictions and the simulation outcomes can be noticed, also by recalling that (10) is the result of a worst case analysis.

If it is relatively easy to discriminate a converging solution from a diverging one, numerical errors can affect the detection of limit cycles. Therefore it has been empirically assumed that if, at the end of the simulation, $\dot{\xi}$ is below the threshold of 0.01 encoder ticks per sample, the system converged to the equilibrium. Also in this case,

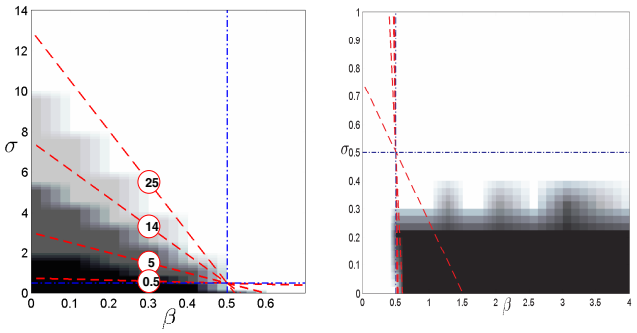

(a) Unstable Behavior (b) Limit Cycles

Fig. 5. Unstable (left) and oscillating (right): simulation results (shaded areas) and theoretical predictions (dashed lines) for different initial velocities $\dot{\xi}(0)$ (whose values are reported in circles).

the simulations agree with the predictions, as shown in Fig. 5(b), obtained with the same parameters of Fig. 5(a). The fact that (10) comes from a worst case analysis is more evident here, since limit cycles actually happen in a subset of the predicted region. We also notice that the existence of the limit cycle does not depend, in this region, on β and σ; in other words even if the viscous friction is initially well on the right of the critical line, a limit cycle arises.

IV. Passivity Analysis of Digital Springs

The simulation of passive objects (e.g. virtual walls), should be implemented in such a way that unrealistic oscillations that could destroy the illusion of interacting with real objects are avoided. Besides, if both the operator and the haptic display are passive systems, their feedback interconnection of Fig. 2 is still a passive, and therefore globally stable system [12].

The passivity inequality [12] means that only a finite amount of energy can be extracted from the system constituted by the haptic device and its control algorithm. By using the notion of dissipativity introduced by [13] and [12], it is possible to relate the passivity of a system to a positive definite state function $\mathcal{H}_T(\tau) = \mathcal{H}_T(\xi(\tau), \dot{\xi}(\tau))$ representing the stored energy:

$$\int_{\tau_0}^{\tau_1} \varphi_H(\tau)\dot{\xi}(\tau)d\tau \geq \mathcal{H}_T(\tau_1) - \mathcal{H}_T(\tau_0) \quad \forall \tau_1 \geq \tau_0 \quad (12)$$

If we explicitly take into account the power $P_d(\tau)$ that is dissipated because of physical friction and the power $P_g(\tau)$ that is "generated" by the non-idealities in the control loop (*energy leaks* [7]), we have:

$$\int_{\tau_0}^{\tau_1} \varphi_H(\tau)\dot{\xi}(\tau)d\tau = \mathcal{H}_T(\tau_1) - \mathcal{H}_T(\tau_0) + \int_{\tau_0}^{\tau_1} [P_d(\tau) - P_g(\tau)]\, d\tau \quad (13)$$

By comparing (12) to (13), the haptic display is passive iff:

$$\int_{\tau_0}^{\tau_1} P_d(\tau)d\tau \geq \int_{\tau_0}^{\tau_1} P_g(\tau)d\tau \qquad \forall \tau_1 \geq \tau_0 \quad (14)$$

The total energy $\mathcal{H}_T(\xi, \dot{\xi})$ stored in the haptic display is given by the sum of the kinetic energy of the device and of the pseudo-elastic potential energy $\mathcal{H}_e(\xi)$ stored in the quantized spring. To compute $\mathcal{H}_e(\xi)$, we rewrite the relation between the real and the quantized position as:

$$\xi = \lfloor \xi \rfloor + \rho \qquad 0 \leq \rho < 1 \quad (15)$$

where $\rho = \rho(\xi)$ represents the quantization error and is a function exclusively of the position ξ. Note that the static compensation of this error introduced in (5) has the effect to translate vertically the diagram so that the magnitude of the compensated error is bounded by $\frac{1}{2}$, but does not alter the fact that ρ is a positional function. For this reason, $\mathcal{H}_e(\xi)$ is expressed by:

$$\mathcal{H}_e(\xi) = -\int \varphi_V(\xi)d\xi = \frac{1}{2}\xi^2 + \frac{1}{2}\left(\rho(\xi) - \rho^2(\xi)\right) \quad (16)$$

where the term depending on $\rho(\xi)$ is always positive because $\rho \in [0; 1[$. Finally $\mathcal{H}_T(\xi, \dot{\xi})$ is given by:

$$\mathcal{H}_T(\xi, \dot{\xi}) = \frac{1}{2}\mu\dot{\xi}^2 + \frac{1}{2}\left(\xi^2 + \rho(\xi) - \rho^2(\xi)\right) \quad (17)$$

A. Energy Leaks

Previous works [3], [6], [7] showed that energy generation for a time discrete, non quantized virtual spring occurs because of the time-delay due to the zero-order-hold (see Fig. 2). Indeed, the force/displacement diagram of a time discrete spring shows that a negative hysteresis loop arises, whose area represents the net amount of energy that is generated. If we analyze the corresponding diagram of a time-continuous, quantized spring, however, we note that the compression and the restitution phases generate exactly overlapping diagrams, because the quantization is a purely positional function. Therefore we can conclude that energy is not generated nor dissipated, even if the diagram differs from that one of a physical spring, and quantization does not cause energy leaks.

In the time discrete case, however, the quantization error plays a role. Indeed, depending on the position when sampling occurs, it happens that the generated energy can be larger or smaller than in the non-quantized case. Therefore quantization can affect the overall energy balance and a worst case analysis is required.

The time discretization is associated to energy generation for the system of Fig. 2. The amount of energy $E_g(\tau_0, \tau_1)$ that is generated during the time interval $\tau \in [\tau_0; \tau_1[$ can be computed by comparing the energy variation of the digital spring (5) to its time continuous counterpart that exerts the force $\varphi(\tau) = -\lfloor \xi(\tau) \rfloor - \frac{1}{2}$:

$$E_g(\tau_0,\tau_1) = \int_{\tau_0}^{\tau_1} P_g(\tau)d\tau = \int_{\tau_0}^{\tau_1} [\varphi_V(\tau) - \varphi(\tau)]\, \dot{\xi}(\tau)d\tau \quad (18)$$

Note that this approach is similar to what followed in [8] and therefore the obtained results could be easily extended the multidimensional case accounting for additional time delays introduced e.g. by the complexity of the virtual environment and by the settling time of the actuators.

Since the passivity inequality (14) has to be satisfied for every $\tau_1 \geq \tau_0$, we can initially suppose that both τ_0 and τ_1 belong to the same sampling interval (i.e. $\tau_0,\ \tau_1 \in$

$[h;(h+1)[$), and then extend the result obtained to every $h \in \mathbb{N}$. In this way, $\varphi_V(\tau)$ is constant over the integration interval and therefore (18) can be rewritten as:

$$E_g(\tau_0,\tau_1) = \frac{1}{2}\Big[\xi(\tau_1)-\xi(\tau_0)\Big]^2 + E_{gq}(\tau_0,\tau_1) \qquad (19)$$

where the first term is always positive and represents the energy generated in the non-quantized case while the latter, recalling (15) and assuming $\rho_0 = \rho(\xi(\tau_0))$, $\rho_1 = \rho(\xi(\tau_1))$ for notational simplicity, is defined as:

$$E_{gq}(\tau_0,\tau_1) = \left(\rho_0-\frac{1}{2}\right)\Big(\lfloor\xi(\tau_1)\rfloor-\lfloor\xi(\tau_0)\rfloor\Big)-\frac{1}{2}\Big(\rho_1-\rho_0\Big)^2 \qquad (20)$$

and represents the effect of position quantization.

It is easy to recognize that, according to what previously observed, E_{gq} can be either positive or negative. Since $\rho(\tau)$ and $\lfloor\xi(\tau)\rfloor$ are independent quantities, it is possible now to compute the maximum of $E_{gq}(\tau_0,\tau_1)$ with respect to ρ_0 and ρ_1. Remembering that $\rho \in [0;1[$, (20) we have:

$$E_{gq}(\tau_0,\tau_1) \le \frac{1}{2}\Big|\lfloor\xi(\tau_1)\rfloor-\lfloor\xi(\tau_0)\rfloor\Big| = \frac{1}{2}\Big|\xi(\tau_1)-\xi(\tau_0)\Big| \qquad (21)$$

because the maximum is reached, depending on the sign of the displacement, when $\rho_0{=}\rho_1{=}0$ or $\rho_0{=}\rho_1{=}1$.Therefore, by recalling (19) we can state that the energy that is generated during the considered time interval is upperly bounded by:

$$E_g(\tau_0,\tau_1) \le \frac{1}{2}\Big[\xi(\tau_1)-\xi(\tau_0)\Big]^2 + \frac{1}{2}\Big|\xi(\tau_1)-\xi(\tau_0)\Big| \qquad (22)$$

B. Energy Dissipation

In the model (1) of the haptic interface, we took into account two main dissipative phenomena: viscous friction, modeled by the dimensionless parameter β, and the dynamic Coulomb friction σ. This modeling choice corresponds to a worst case scenario with respect to friction. Indeed, especially at low velocities, other phenomena like static Coulomb friction, Stribeck friction generally add other dissipation, thus helping the system to preserve its passivity, even if the overall transparency is affected.

By computing the amount of energy dissipated $E_d(\tau_0,\tau_1)$ by (6) during the same time interval considered above, we have:

$$E_d(\tau_0,\tau_1) = \int_{\tau_0}^{\tau_1} P_d(\tau)d\tau = \int_{\tau_0}^{\tau_1}\Big[\beta\dot\xi^2(\tau)+\sigma|\dot\xi(\tau)|\Big]d\tau \qquad (23)$$

A lower bound on $E_d(\tau_0,\tau_1)$ has to be computed in order to carry out a worst case analysis on the energy dissipation. For the term due to the dynamic Coulomb friction we have:

$$\int_{\tau_0}^{\tau_1}\sigma\Big|\dot\xi(\tau)\Big|d\tau \ge \sigma\left|\int_{\tau_0}^{\tau_1}\dot\xi(\tau)d\tau\right| = \sigma\Big|\xi(\tau_1)-\xi(\tau_0)\Big| \qquad (24)$$

while for the viscous friction the Cauchy-Schwarz inequality gives:

$$\left(\int_{\tau_0}^{\tau_1}\dot\xi^2(\tau)d\tau\right)^{\frac{1}{2}}\left(\int_{\tau_0}^{\tau_1}1^2d\tau\right)^{\frac{1}{2}} \ge \left|\int_{\tau_0}^{\tau_1}1\dot\xi(\tau)d\tau\right|$$

$$\Longrightarrow \int_{\tau_0}^{\tau_1}\beta\dot\xi^2(\tau)d\tau \ge \beta\frac{\Big[\xi(\tau_1)-\xi(\tau_0)\Big]^2}{\tau_1-\tau_0} \qquad (25)$$

and finally the sum of (24) and (25) expresses the lower bound on the the total dissipated energy energy:

$$E_d(\tau_0,\tau_1) \ge \beta\frac{\Big[\xi(\tau_1)-\xi(\tau_0)\Big]^2}{\tau_1-\tau_0} + \sigma\Big|\xi(\tau_1)-\xi(\tau_0)\Big| \qquad (26)$$

C. Passivity Condition

The passivity condition (14) has to be satisfied for every $\tau_1{>}\tau_0$, therefore the minimum amount of dissipated energy has to be larger than the maximum amount of generated energy during the same time interval. Hence, by using (22) and (26):

$$\left(\beta-\frac{1}{2}\right)\frac{\Big[\xi(\tau_1)-\xi(\tau_0)\Big]^2}{\tau_1-\tau_0}+\left(\sigma-\frac{1}{2}\right)\Big|\xi(\tau_1)-\xi(\tau_0)\Big| \ge 0 \qquad (27)$$

Since we assumed both τ_0 and τ_1 belonging to the same sampling interval, we have that $\tau_1-\tau_0 \le 1$. Because of the continuity of the velocity $\dot\xi(\tau)$ the mean value theorem holds, leading to:

$$|\xi(\tau_1)-\xi(\tau_0)| = |\dot\xi(\tau)|(\tau_1-\tau_0) \le |\dot\xi(\tau)|; \quad \tau_0<\tau<\tau_1 \qquad (28)$$

Finally, by substituting into (27), we obtain the passivity condition (8). As noted in [3], the sufficiency of this condition holds also when the unilateral constraint representing the virtual wall is considered. Indeed, the device is passive when φ_V is null and, when it is moving the dissipation provided by intrinsic friction is larger than energy generation. Therefore the virtual force φ_V can be set to zero at any time without affecting the energy balance.

V. Experimental Results

Experimental validation of the proposed criterion has been carried out by means of a Maxon RE35 motor equipped by an encoder having 8192 counts per revolution; since it is a rotative device, positions and forces in (1) correspond to angles and torques. A Copley 403 amplifier was used and commanded via a 14 bit D/A interface from the Linux-RTAI control loop. The actual encoder resolution and the sampling time can be changed in the control software, in this way we can test different points on the (β,σ) plane, according to what sketched in Fig. 4.

The estimation of friction parameters of the device leads to $b{=}9{\times}10^{-6}$ Nm/rad sec, $c{=}2{\times}10^{-3}$ Nm and $m{=}6.28{\times}10^{-6}$ Kg m^2; since in this case the Coulomb dynamic friction is much larger than the viscous friction, the device is likely to operate in the locally stable/unstable region (see Fig. 3).

The initial velocity appearing in (10) is difficult to measure. Therefore, to obtain more precise data, the initial velocity has been converted into an initial displacement for the virtual spring in such a way that the energy $\mathcal{H}_T(\xi,\dot\xi)$ initially stored in the haptic display is the same. Fig. 6(a) through 6(d) show the outcomes obtained with points in each of the four regions of the (β,σ) plane. On the left of each figure it is shown the characteristic point and the critical line associated to the initial condition, while on the

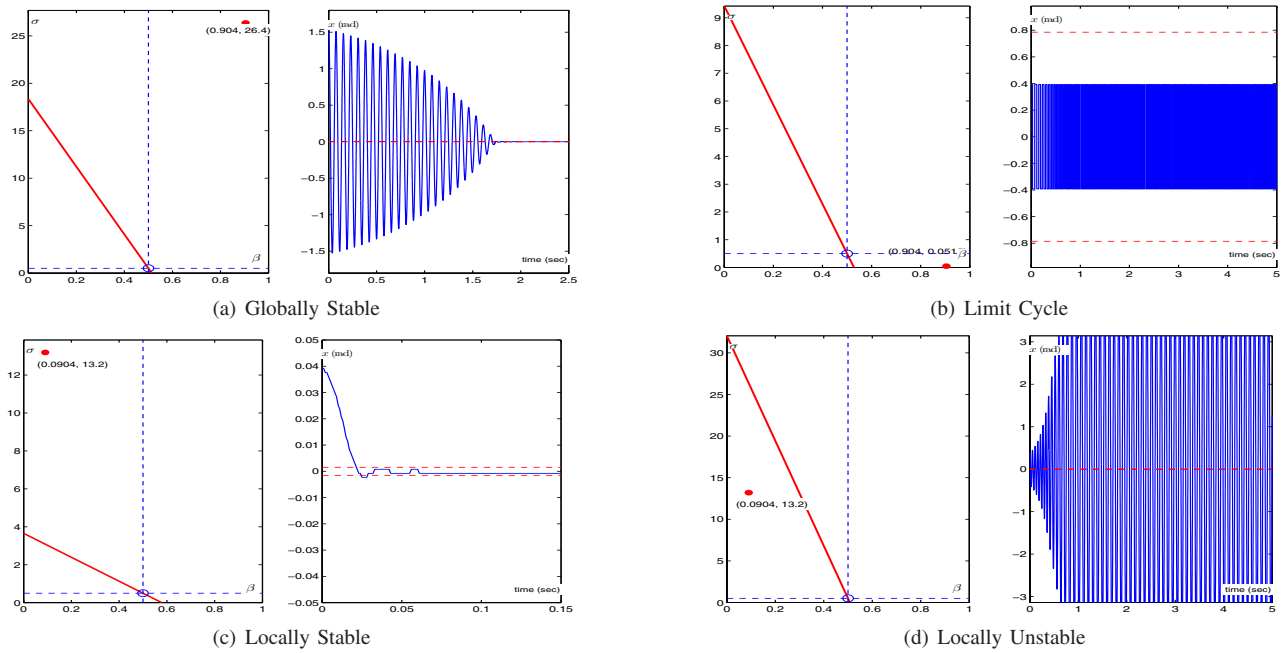

(a) Globally Stable (b) Limit Cycle

(c) Locally Stable (d) Locally Unstable

Fig. 6. Characteristic point and initial condition on the (β, σ) plane and position vs. time for different operating conditions.

right it is shown the temporal diagram of the angular displacement; in this same diagram the dashed horizontal lines correspond to ± 1 encoder tick. Starting from Fig. 6(a), we evaluated a point located in the globally stable region and, despite the high initial condition represented by the slope of the critical line, the position converges to the origin. Then, by simulating a very poor encoder resolution, the behavior of a point located in the limit cycles region is investigated, (Fig. 6(b)) and, as predicted, we observe a persistent oscillation bounded by the encoder resolution. By changing the initial conditions, the behavior of a point located in the locally stable region have been finally studied, Fig. 6(c) and 6(d). As expected, by increasing the initial energy stored into the digital spring, the system becomes unstable.

VI. Conclusions

The dimensionless formulation of the model (1) allowed a simple passivity analysis of the haptic interface, leading to a general passivity criterion relating the intrinsic viscous and Coulomb friction of the device to the displayed stiffness, sampling time and encoder resolution. In particular, it has been shown that, depending on the initial velocity, stable interactions can be obtained even if the effective viscous friction is small. Moreover, the criterion can be used as a guideline in the dimensioning of the components of a haptic device, establishing the motor parameters, encoder resolution, and servo rate necessary to achieve the desired stiffness.

In future work, we plan to expand the results to include the amplifier's bandwidth limitations as well as the motor's current limits. Also, we hope to utilize the findings to create improved control algorithms which may adapt stiffness to the device velocity or add virtual damping to remove excess energy explicitly, ultimately providing better and more robust haptic interfaces.

References

[1] T. Massie and J. Salisbury, "The phantom haptic interface: a device for probing virtual objects," in *ASME Winter Annual Meeting*, vol. 55-1, New Orleans, LA, 1994, pp. 295–300.

[2] F. Barbagli and J. Salisbury, "The effect of sensor/actuator asymmetries in haptic interfaces," in *IEEE Haptics Symposium*, Los Angeles, CA, March 2003, pp. 140–147.

[3] J. Colgate and G. Schenkel, "Passivity of a class of sampled-data systems: Application to haptic interfaces," in *American Control Conference*, Baltimore, Maryland, June 1994, pp. 3236–3240.

[4] B. Hannaford and J. Ryu, "Time domain passivity control of haptic interfaces," in *Proceedings of the IEEE International Conference on Robotics and Automation*, Seoul, Korea, May 2001, pp. 1863–1869.

[5] N. Hogan, "Controlling impedance at the man/machine interface," in *Proceedings IEEE International Conference on Robotics and Automation*, 1989, pp. 1626–1631.

[6] J. Colgate, P. Grafing, M. Stanley, and G. Schenkel, "Implementation of stiff virtual walls in force-reflecting interfaces," in *IEEE Virtual Reality Symposium*, 1993, pp. 202–208.

[7] B. Gillespie and M. Cutkosky, "Stable user-specific rendering of the virtual wall," in *ASME IMECE*, vol. DSC-Vol. 58, Atlanta, GA, November 1996, pp. 397–406.

[8] M. Mahvash and V. Hayward, "High fidelity passive force reflecting virtual environments," *IEEE Transactions on Robotics*, 2004, in press.

[9] M. Kawai and T. Yoshikawa, "Haptic display with an interface device capable of continuous-time impedance display within a sampling period," *IEEE/ASME Transactions on Mechatronics*, vol. 9, no. 1, pp. 58–64, March 2004.

[10] J. Hwang, M. Williams, and G. Niemeyer, "Toward event-based haptics: Rendering contact using open-loop force pulses," in *Proc. IEEE 12th International Symposium on Haptic Interfaces for Virtual Environment and Teleoperator Systems (HAPTICS' 04)*, March 2004, pp. 24–31.

[11] S.Stramigioli, C.Secchi, A. van der Schaft, and C. Fantuzzi, "A novel theory for sample data system passivity," in *Proceedings of the IEEE/RSJ International Conference on Intelligent Robots and Systems*, Lausanne, Switzerland, October 2002.

[12] A. van der Schaft, *L_2-Gain and Passivity Techniques in Nonlinear Control*, ser. Communication and Control Engineering. Springer Verlag, 2000.

[13] J. Willems, "Dissipative dynamical systems, part i: General theory," *Arch. Rat. Mech. An.*, vol. 45, 1972.